

Friction Study of a Ni Nanodot-patterned Surface

Hengyu Wang · Rahul Premachandran Nair · Min Zou · Preston R. Larson ·
Andrew L. Pollack · K. L. Hobbs · Mathew B. Johnson · O. K. Awitor

Received: 15 June 2007 / Accepted: 6 August 2007 / Published online: 21 August 2007
© Springer Science+Business Media, LLC 2007

Abstract Nanoscale frictional behavior of a Ni nanodot-patterned surface (NDPS) was studied using a TriboIndenter by employing a diamond tip with a 1 μm nominal radius of curvature. The Ni NDPS was fabricated by thermal evaporation of Ni through a porous anodized aluminum oxide (AAO) template onto a Si substrate. Surface morphology and the deformation of the NDPS were characterized by scanning electron microscopy (SEM) and atomic force microscopy (AFM), before and after friction/scratch testing. SEM images after scratching clearly showed that, similar to what was assumed at the macroscale, the frictional force is proportional to the real area of contact at the nanoscale. It was found that adhesion played a major role in the frictional performance, when the normal load was less than 20 μN and plastic deformation was the dominant contributor to the frictional force, when the normal load was between 60 μN and 125 μN . Surprisingly, a continuum contact mechanics model was found to be applicable to the nanoscale contact between the tip and the inhomogeneous Ni NDPS at low loads. The coefficient of friction (COF) was also found to depend on the size of the tip and was four times the COF between a 100 μm tip and the Ni NDPS. Finally, the critical shear strength of the Ni

nanodots/Si substrate interface was estimated to be about 1.24 GPa.

Keywords Friction · Nanoscale · Nickel · Nanodot-patterned surface · Nano-patterning · Anodized aluminum oxide (AAO)

1 Introduction

Friction is a phenomenon that has been studied for centuries since the early days of Leonardo da Vinci (1452–1519). Amontons' law, which states that friction is proportional to the normal load, has described many macroscopic and microscopic non-adhesive sliding contacts, surprisingly well [1, 2]. For miniaturized systems, such as micro-electro-mechanical systems/nano-electro-mechanical systems (MEMS/NEMS), however, Amontons' law no longer applies, because the adhesion contribution to friction can no longer be neglected due to the large surface-area-to-volume ratio of MEMS/NEMS structures and the increased surface smoothness [3]. In fact, adhesion and friction are two of the main issues affecting the reliability of MEMS/NEMS devices involving contact interfaces [4]. Therefore, a fundamental understanding of friction at nanoscale dimensions and controlling friction through nano-surface-engineering are of great scientific and technological significance.

Recently, surface nano-patterning with Ni nanodot arrays on a Si substrate was investigated for adhesion and friction reduction of contacting interfaces for potential tribological applications in miniaturized systems [5]. The results showed that the adhesion forces and the coefficients of friction (COF) between a 100 μm diamond tip and the Ni nanodot-patterned surface (NDPS) were reduced up to

H. Wang · R. Premachandran Nair · M. Zou (✉)
Department of Mechanical Engineering, University of Arkansas,
Fayetteville, AR 72701, USA
e-mail: mzou@uark.edu

P. R. Larson · A. L. Pollack · K. L. Hobbs · M. B. Johnson
Department of Physics & Astronomy, University of Oklahoma,
Norman, OK 73019, USA

O. K. Awitor
Département Mesures, Physiques, Université d'Auvergne,
Clermont, France

92% and 83%, respectively, compared to those of a smooth silicon surface. Detailed frictional studies suggest that adhesion played a major role in the friction performance when the normal load was small. The nanoscale multi-asperity contact between the diamond tip and inhomogeneous Ni NDPSs under low loads was found to follow a continuum contact mechanics model. Another tribology study of a silica nanoparticle-textured surface [6], however, showed that the friction performance of the nano-textured surface depended on the radius of curvature of the tip used to measure the friction. The texture benefit was realized only when the tip size was relatively large compared to the texture spacing. For a better understanding of the effect of tip size on the frictional behavior of the Ni NDPS so as to provide design guidelines for minimizing friction for NDPSs, this article focuses on studying the frictional behavior of a 1 μm diamond tip sliding on the Ni NDPS.

2 Experimental

2.1 Sample Preparation

The Ni NDPS was fabricated by thermal evaporation of Ni through a porous anodic aluminum oxide (AAO) template onto a Si substrate, as described in detail elsewhere [5]. The resulting pattern, which was roughly 3 mm \times 3 mm in size, consisted of a well-ordered hexagonal array of 75 nm tall conical shaped Ni dots approximately 75 nm in diameter at the base with a dot-to-dot separation of 100 nm.

Next, alignment markers were fabricated on the Ni NDPS using photolithography. These markers were designed to aid the placement of the scratches for friction/scratch testing and to facilitate the locating of the scratches for scanning electron microscope (SEM) and atomic force microscopy (AFM) characterizations after the friction/scratch testing.

2.2 Sample Topography and Tribological Characterizations

Sample topography characterization before and after friction/scratch testing were performed using a JEOL JSM-880 SEM and a Topometrix Explorer AFM. Friction/scratch investigations were conducted in air at a relative humidity of about 40% using a Hysitron TriboIndenter that has force and displacement sensing capabilities in both vertical and lateral directions. The sensing system in the TriboIndenter consists of two three-plate capacitive force-displacement transducers with integrated electrostatic actuation functionality. The resolution is 0.02 nm for vertical displacement, 3 nN for vertical/indentation force, and

500 nN for lateral force. The TriboIndenter also has an optical microscope that allows one to easily locate the alignment markers and Ni nanodot-patterned areas for friction/scratch testing. The tip used in the friction/scratch study was a conical diamond tip with nominal radius of curvature of 1 μm .

The friction/scratch tests were conducted using a ramp load profile from 0 μN to 10 different maximum normal loads (10–500 μN) at a sliding speed of 1 $\mu\text{m/s}$ with 8 μm scratch lengths. The friction/scratch tests consisted of seven steps: (1) the tip engaging the sample surface at a contact force of about 1 μN in the mid point of the expected scratch, (2) the tip sliding toward one end of the expected scratch in 4 s under zero normal load, (3) the tip staying at this end of scratch for 5 s under zero normal load, (4) the tip scratch toward the other end of the expected scratch in 8 s under the desired ramp normal load, (5) the tip staying at the end of the scratch for 5 s while the normal load is reduced to zero, (6) the tip moving back to the middle of the scratch under zero normal load, and (7) the tip withdrawing from the sample surface. The purpose of employing steps (1) and (2) was to properly account for the sample tilt in the normal displacement data collected. The time allowed in step (3) was to minimize any dynamic effects from step (2). The friction/scratch tests were repeated three times for each ramp load profile. The normal and lateral displacements and forces were recorded simultaneously and continuously as a function of time during sliding for each test. The COF was calculated as the ratio of the measured lateral force and applied normal force during tip sliding in step (4).

3 Results and Discussion

3.1 Ni Nanodot-patterned Surface Characterization

Figure 1a shows a top down SEM micrograph of the well-ordered array of Ni nanodots. The hexagonal arrangement of the dots resulted from the hexagonal pore structure in the AAO template mask and exhibits good ordering over micron-sized domains. The inset in the upper right hand corner of Fig. 1a shows a 45° oblique angle view of the Ni NDPS illustrating the conical shape of the dots. Figure 1b shows the top down view of an AFM image of the Ni NDPS. From Fig. 1 and other representative SEM and AFM images, the height, base diameter, and dot-to-dot spacing were found to be 75, 75, and 100 nm, respectively.

3.2 Frictional Behavior of the NDPS

Figure 2 shows the COF as a function of the normal load for four out of the 10 different scratch tests: 0–40 μN ,

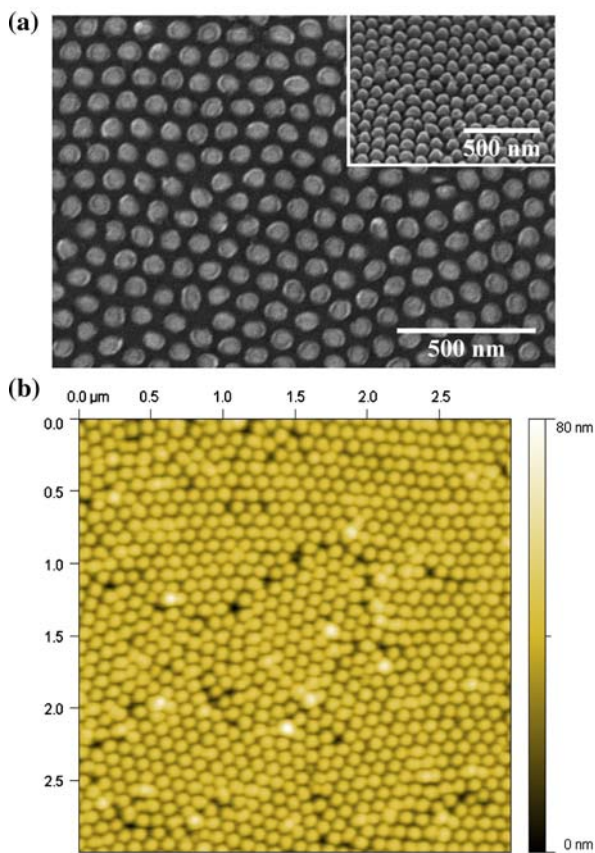
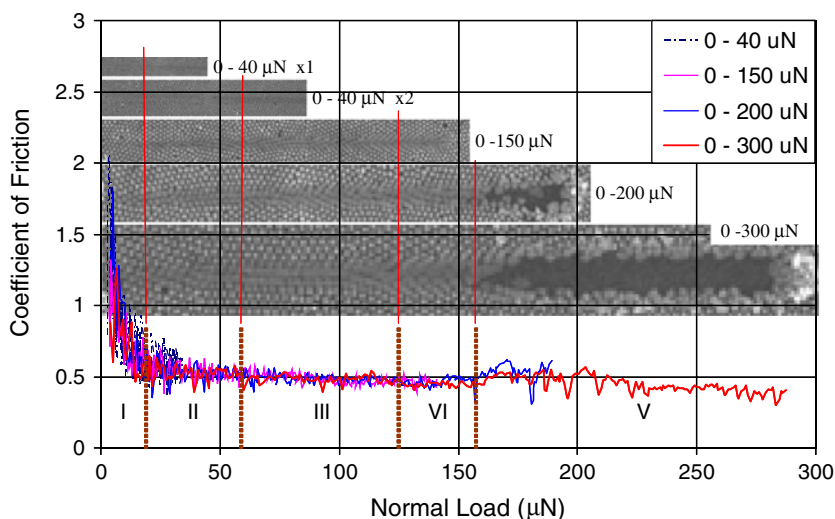


Fig. 1 SEM and AFM images of the Ni NDPS: (a) SEM top down view. Inset in upper right hand corner shows a 45° oblique angle view of the Ni dots; (b) AFM top down view

0–150 μN , 0–200 μN , and 0–300 μN . The four scratch tests were selected to cover both low load and high load ranges with sufficient data collection resolution and to clearly show the general trends of the COFs versus normal loads. The inserted SEM micrographs show the corresponding deformations of the sample surfaces after the

Fig. 2 Coefficient of friction as a function of normal load for four different scratch tests: 0–40 μN , 0–150 μN , 0–200 μN , and 0–300 μN . The inserted SEM micrographs show the corresponding deformations of the sample surfaces after the scratch tests

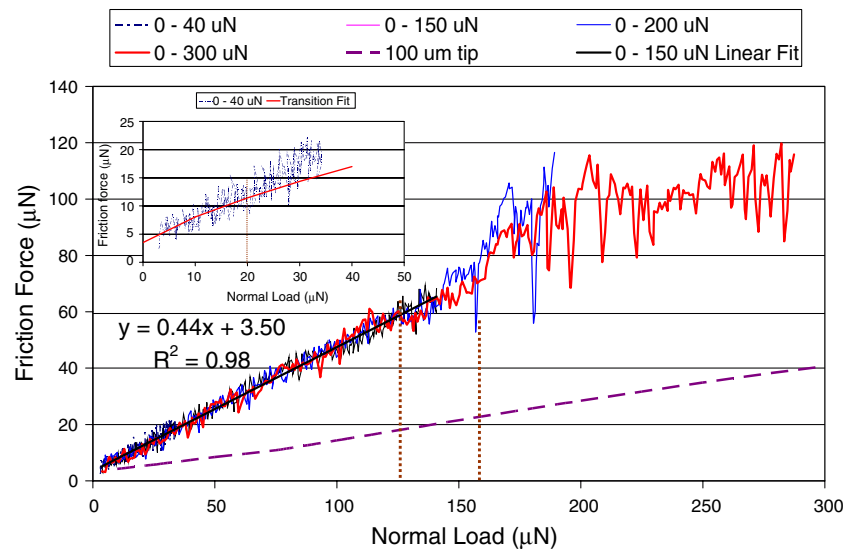


scratch tests. It can be seen that the COF was not a constant as predicted by Amontons’ law. The COF as a function of normal load can be divided into the following five regimes: (I) the COF was relatively high when the normal load was less than 20 μN , (II) the COF approached a constant value of about 0.5 from 20 μN to 60 μN normal load, (III) the COF remained relatively constant at 0.5 until the normal load reached 125 μN , (IV) the COF slightly decreased between 125 μN and 160 μN normal load, and (V) the COF became erratic when the normal load was larger than 160 μN .

The non-constant behavior of the COF versus normal load can be attributed to different friction mechanisms. At low load (regime I), the contribution from the adhesion force between the tip and NDPS to the friction force can not be neglected as shown in Fig. 3, which shows the frictional force as a function of the normal load for the four scratch tests presented in Fig. 2. It can be seen that even though there was a good linear fit when the normal load was less than 125 μN , the fitted line did not go through the origin as predicted by Amontons’ law. In other words, the frictional force was not zero when the normal load was zero. Instead, the frictional force at zero normal loads was about 3.5 μN due to the adhesion force.

A theory of continuum contact mechanics was employed to quantify the relationship between the frictional force and the applied normal load for loads smaller than 40 μN . Continuum contact mechanics models have been applied to nanotribology measurements to determine fundamental parameters and processes in nanometer-scale single-asperity contacts for the past 15 years [7]. An increasing amount of data supports the conclusion that a continuum description of contact is sometimes accurate down to nanometer-sized single-asperity contacts. This is particularly surprising because many of the basic assumptions associated with these continuum contact mechanics

Fig. 3 Frictional force and normal load relationships for four different nominal normal loads. Inset plot shows the frictional force and normal load relationship at low load fitted with the transition model



models, such as homogeneous, isotropic and linear elastic materials, and the contact radius being much smaller than the radius of curvature of the contacting interfaces, are violated for many of the interfaces studied. Several adhesive continuum contact mechanics theories have been developed based on Hertzian theory [8]. These theories consider attractive forces between the contacting asperities. The Johnson–Kendall–Roberts (JKR) theory [9] and the Derjaguin–Muller–Toporov (DMT) theory [10] represent opposite ends of the spectrum of a nondimensional transition parameter (representing the ratio of the normal elastic deformation caused by adhesion to the effective range of the adhesion forces). Generalization of these two limiting cases to an intermediate case applicable to an actual interface interaction was achieved by Maugis using a Dugdale model in continuum fracture mechanics [11], and further simplified by Carpick et al. using a generalized transition model [12].

In the plot inset in Fig. 3, the frictional force versus normal load data was plotted for normal loads less than 40 μN . Also plotted was the fitted data using a continuum contact mechanics model, according to a procedure described by Grierson et al. [7]. First, the appropriate continuum contact model was determined from the measured average adhesion force at 10 μN indentations. We took the value of the Young’s modulus for Ni and diamond as 200 GPa and 1141 GPa, respectively, and the Poisson’s ratio for Ni and diamond as 0.31 and 0.07, respectively. We also assumed the value of the effective range of adhesion for the Ni NDPS to be 0.234 nm, which is the Ni–Ni bond distance. The transition parameters obtained from these values are 0.64, which is larger than 0.1 and less than 5. Therefore, the tip/Ni NDPS interface was determined to be in the transition regime. Second, we fit the frictional force versus normal load curves using the generalized transition

model [12]. From the inset in Fig. 3, it can be seen that the generalized transition model fits the experimental data very well for normal loads less than 20 μN , again suggesting the adhesion force contribution to the frictional force is significant at loads less than 20 μN .

The applicability of the continuum contact mechanics model to the nanoscale multi-asperity contact between a 100- μm diamond tip and the Ni NDPS has been previously observed [5]. The elastic contact model applies to each Ni dot/tip interface if the contact interface materials are homogeneous and only elastic deformation occurs. Since the Ni NDPS (a combination of nanometer-sized Ni dots and the Si substrate) is inhomogeneous and plastic deformation occurred at low loads in this study (shown later in Sect. 3.3), it is again very interesting to see that the classical contact mechanics model can still be used to explain the nanoscale contact. The reason for this is not fully understood yet and will be the subject of future study.

At higher loads (regime III), Fig. 2 shows that the COFs were nearly independent of the normal loads. In these cases, the dominant deformation process was plastic shearing (plowing) of the nanodots on the surface by the diamond tip as shown by the inserted SEM micrographs. When the shearing (plowing) mechanism prevails over adhesion, the COF depends primarily on the shape of the hard asperity (diamond tip) and the shear strength (or hardness) of the plowed material (Ni NDPS) [13–15], and thus the COF remained constant. Regime II represents a transition regime, where both adhesion and plastic deformation mechanisms were present. The inserted SEM images show that in regime IV, the Ni nanodots were sheared severely and started loosening from the substrates. In regime V, the Ni nanodots were completely removed from the substrates, and caused the COF to increase suddenly and behaved erratically afterward.

The friction versus load relationship between a 100 μm tip and the Ni NDPS obtained from a previous study [5] was also plotted in Fig. 3 for comparison. It can be seen that the COF between the 1 μm tip and the Ni NDPS (slope of the curve) was about four times the COF between the 100 μm tip and the Ni NDPS. Possible reasons for the much larger COF between the 1 μm tip and the Ni NDPS are: (1) larger plastic deformations due to higher contact pressures at the interface that resulted from a smaller number of nanodots in contact, (2) interlocking between the 1 μm tip and the Ni nanodots, and (3) larger real area of contact between the 1 μm tip and the NDPS. The fact that the SEM micrograph showed dot flattening under a large range of load suggests that the interlocking is not the major mechanism. The SEM micrographs of the scratches produced by the 1 μm tip showed much smaller deformation track widths than the scratches produced by the 100 μm tip, therefore invalidating the real area of contact argument. Therefore, it was concluded that plastic deformation is the main reason for the large COF of the 1 μm tip. This result suggests that the relative size of the asperities of the mating surfaces affect the COF significantly through the contact area and pressure change. NDPSs can be used to reduce friction only when the asperities of the mating surfaces are relatively large compared to the spacing among the nanodots.

3.3 Deformation of the Ni NDPS

Detailed SEM investigations were conducted to reveal the deformations of the NDPS after scratching under different normal loads. Figure 4 shows an example of SEM analysis on a low load 0–40 μN scratch. Four SEM micrographs with different magnifications were presented. Figure 4a shows the unprocessed 7kx SEM micrograph, on which the scratch can hardly be seen. However, after adjusting the brightness and contrast of the original SEM micrograph, the scratch is clearly shown in Fig. 4b. In order to show the Ni nanodot deformation better, SEM micrographs were taken at higher magnifications, and are shown in Fig. 4c, d. It can be seen from Fig. 4c that the Ni nanodots deformed plastically even at very small normal loads at the beginning of the scratch, shown as the color contrast in the micrograph. The plastic deformations of the Ni nanodots at loads greater than 20 μN were clearly shown by the altered shapes of the dots. The real area of contact, shown in Fig. 4b in between the dotted lines, increased linearly with the applied normal load. Since, Fig. 3 shows that the frictional force was proportional to the normal load when the normal load was less than 40 μN we concluded that the frictional force was proportional to the real area of contact as generally assumed for macroscale friction.

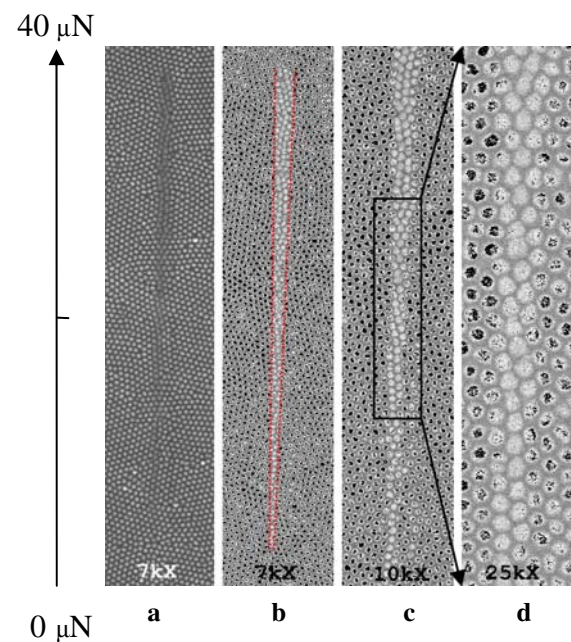
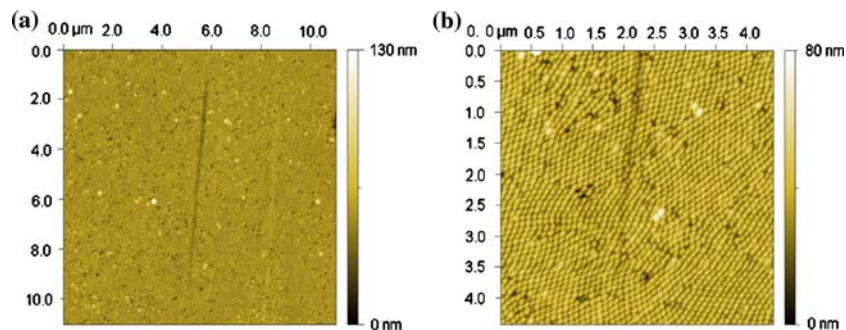


Fig. 4 SEM micrographs illustrating the deformations of the Ni dots after a 0–40 μN scratch test: (a) Unprocessed micrograph; (b) adjusted micrograph brightness and contrast to show the scratch better; (c, d) higher magnification micrographs

AFM measurements were taken to further quantify the deformation of the Ni NDPS in the height direction under different normal loads. The two AFM images in Fig. 5 show the deformations of the Ni NDPS after a 0–20 μN scratch test. Figure 5(a) is a lower resolution image showing the whole scratch and (b) is a higher resolution image showing the beginning end of the scratch. (Note that the scratch starts from the bottom of the figure). Characterization results showed that at the beginning of the scratch only one or two Ni nanodots were in contact with the tip and the scratch test caused the Ni nanodots to deform plastically in the whole length of the scratch. Cross-sectional line scans revealed that even at the very beginning of the scratch, the Ni nanodots were deformed about 5–10 nm in the height direction. The estimated maximum shear stress for a single asperity contact under 4 μN normal load, which was the actual normal load applied at the beginning of the scratch instead of 0 μN specified due to the imprecision of the TriboIndenter, was 8.4 GPa assuming the Hertz contact model without lateral force [8]. This shear stress is much larger than the theoretical shear strength of Ni of 2.6 GPa [16], which therefore caused the Ni dot to deform readily. However, the minute deformations under such a high contact pressure indicate the unusual strength of the Ni nanodots.

Fig. 5 AFM images showing the deformations of the Ni dots after a 0–20 μN scratch test: (a) lower resolution image showing the whole scratch; and (b) higher resolution image showing the beginning end of the scratch



3.4 Critical Shear Strength of the Ni Nanodots/Si Substrate Interface

The frictional force versus the lateral displacement curve contains a wealth of information regarding the deformation behavior of the NDPS and the critical shear strength of the Ni nanodots/Si substrate interface. Figure 6 shows the relationship between the frictional force and the lateral displacement for a 0–200 μN scratch along with the SEM micrograph of the surface after the scratch. It can be seen that there is a good correlation between the frictional force and the surface deformation. The five regimes identified in Fig. 2 can also be seen in Fig. 5 with the aid of the SEM micrograph that provided evidence of different deformations in each regime. The SEM micrograph shows that only slight plastic deformation of Ni nanodots occurred in regime I and transitioned to a larger plastic deformation in regime II. In regime III, significant dots flattening was observed. Finally, in regime IV, the dots became loose and

were completely removed in regime V. The frictional force versus lateral displacement curve showed clear indications at the transitions from one regime to the other.

The critical shear strength of the Ni nanodots/Si substrate interface was estimated from the shear stress at which the Ni nanodots were removed from the silicon substrate. By examining the lateral force and SEM micrographs of the scratch together, we found that the critical shear stress point corresponds to the point when the lateral force becomes irregular (critical lateral force). Therefore, the critical shear stress of the Ni nanodots/Si substrate interface was calculated by dividing the critical lateral force by the area of contact between the tip and the NDPS at the critical lateral force determined from the SEM micrographs of the scratch. Table 1 shows the critical shear stress at the Ni nanodots removal for 9 different scratches, which gave an average of 1.24 GPa and a standard deviation of 0.01 GPa. This shear stress is very close to the reported value of 1.4 GPa for the Ni/silica interface [17].

Fig. 6 The correlation between surface topography and the signatures in the lateral force versus lateral displacement curve for a 0–200 μN scratch

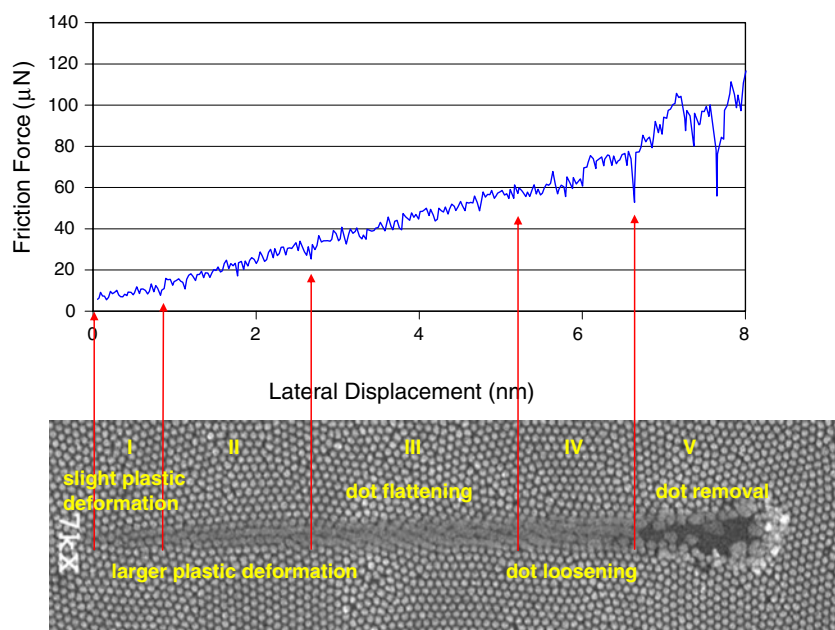


Table 1 The critical shear stresses at which the Ni nanodots were removed from the silicon substrates

Load (μN)	Test #	Lateral force (μN)	No. of dots in contact from SEM	Contact area (μm^2)	Critical shear stress (GPa)
0–200	1	60.0	8.5	0.0482	1.24
	2	70.0	10.0	0.0567	1.23
	3	60.0	8.5	0.0482	1.24
0–300	1	65.0	9.2	0.0522	1.25
	2	90.0	13.0	0.0738	1.22
	3	70.0	10.0	0.0567	1.23
0–400	1	60.0	8.5	0.0482	1.24
	2	73.0	10.5	0.0596	1.23
	3	78.0	11.0	0.0624	1.25
Mean		69.6	9.9	0.0562	1.24
Standard deviation		10.0	1.5	0.0084	0.01

4 Conclusions

Nanoscale frictional behavior of the Ni NDPS was studied using a TriboIndenter. The corresponding deformations were investigated using SEM and AFM. SEM images showed that the frictional force is proportional to the real area of contact at the nanoscale. It was found that adhesion played a major role in the frictional performance when the normal load was less than 20 μN and plastic deformation dominated the frictional performance when the normal load was between 60 μN and 125 μN . The nanoscale contact at low loads between the tip and an inhomogeneous material, the Ni NDPS, was found to follow a continuum contact mechanics model. The relative roughness of the mating surfaces was found to determine the magnitude of the COF. Finally, the critical shear strength of the Ni nanodots/Si substrate interface was estimated to be about 1.24 GPa.

Acknowledgments We thank Arkansas Biosciences Institute and the University of Arkansas for major equipment funding support. We also thank the support by NSF under award CMS-0600642 and the support of the Center for Semiconductor Physics in Nanostructures (C-SPIN), an OU/UA NSF-funded MRSEC (DMR-0520550).

References

- Rabinowicz, E.: Friction and Wear of Materials, 2nd edn. Wiley, New York (1995)
- Persson B.N.J., Tosatt E. (eds.): Physics of Sliding Friction. Kluwer Academic Publishers, Dordrecht (1996)
- Corwin, A.D., de Boer, M.P.: Effect of adhesion on dynamic and static friction in surface micromachining. Appl. Phys. Lett. **84**, 2451–2453 (2004)
- Komvopoulos, K.: Adhesion and friction forces in microelectro-mechanical systems: mechanisms, measurement, surface modification techniques, and adhesion theory. J. Adhes. Sci. Technol. **17**, 477–517 (2003)
- Zou, M., Wang, H., Larson, P.R., Hobbs, K.L., Johnson, M.B., Awitor, O.K.: Ni nanodot-patterned surfaces for adhesion and friction reduction. Tribol. Lett. **24**, 137–142 (2006)
- Zou, M., Cai, L., Wang, H.: Adhesion and friction studies of a nano-textured surface produced by spin coating of colloidal silica nanoparticle solution. Tribol. Lett. **21**, 25–30 (2006)
- Grierson, D.S., Flater, E.E., Carpick, R.W.: Accounting for the JKR-DMT transition in adhesion and friction measurements with atomic force microscopy. J. Adhes. Sci. Technol. **19**, 291–311 (2005)
- Johnson, K.L.: Contact Mechanics. Cambridge University Press, New York (1987)
- Johnson, K.L., Kendall, K., Roberts, A.D.: Surface energy and the contact of elastic solids. Proc. R. Soc. Lond. A **324**, 301–313 (1971)
- Derjaguin, B.V., Muller, V.M., Toporov, Yu.P.: Effect of contact deformations on the adhesion of particles. J. Colloid Interf. Sci. **53**, 314–326 (1975)
- Maugis, D.: Adhesion of spheres: The JKR-DMT transition using a dugdale model. J. Colloid Interf. Sci. **150**, 243–269 (1992)
- Carpick, R.W., Ogletree, D.F., Salmeron, M.: A general equation for fitting contact area and friction vs load measurements. J. Colloid Interf. Sci. **211**, 395–400 (1999)
- Suh, N.P., Sin, H.-C.: The genesis of friction. Wear **69**, 91–114 (1981)
- Komvopoulos, K., Saka, N., Suh, N.P.: The mechanism of friction in boundary lubrication. ASME J. Tribol. **107**, 452–461 (1985)
- Saka, N., Suh, N.P.: Plowing friction in dry and lubricated metal sliding. ASME J. Tribol. **108**, 301–313 (1986)
- Courtney, T.H.: Mechanical Behavior of Materials, 2nd edn. McGraw-Hill, New York (2000)
- Agrawal, D.C., Raj, R.: Ultimate shear strengths of copper-silica and nickel-silica interfaces. Mater. Sci. Eng. A **126**, 125–131 (1990)